

AFRPL TR-85-076

AD:

Final Report  
for the period  
October 1983 to  
July 1985

# A Diffuser Heat Transfer and Erosion Code

October 1985

Author:  
G. H. Buzzard

DTIC  
ELECTE  
DEC 18 1985  
S D  
A

AD-A162 436

## Approved for Public Release

Distribution is unlimited. The AFRPL Technical Services Office has reviewed this report, and it is releasable to the National Technical Information Service, where it will be available to the general public, including foreign nationals.

DTIC FILE COPY

## Air Force Rocket Propulsion Laboratory

Air Force Space Technology Center  
Space Division, Air Force Systems Command  
Edwards Air Force Base,  
California 93523-5000

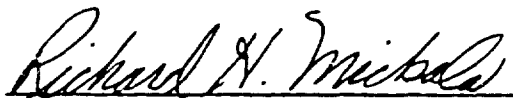
## NOTICE

When U.S. Government drawings, specifications, or other data are used for any purpose other than a definitely related Government procurement operation, the fact that the Government may have formulated, furnished, or in any way supplied the said drawings, specifications, or other data, is not to be regarded by implication or otherwise, or in any way licensing the holder or any other person or corporation, or conveying any rights or permission to manufacture, use, or sell any patented invention that may be related thereto.

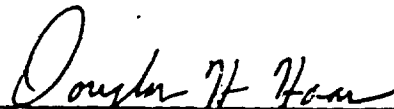
## FOREWORD

This final report, A Diffuser Heat Transfer and Erosion Code, was prepared by Dr Dale H. Buzzard of Duke University as an in-house project while serving as a visiting professor at the Air Force Rocket Propulsion Laboratory (AFRPL), Edwards Air Force Base, California 93523-5000. The AFRPL project manager was Mr Richard Mickola.

This report has been reviewed and is approved for release and distribution in accordance with the distribution statement on the cover and on the DD Form 1473.

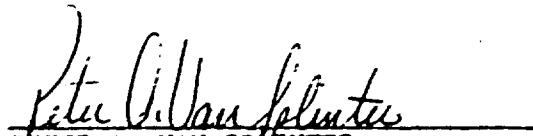


RICHARD H. MICKOLA  
Project Manager



DOUGLAS H. HAAS  
Chief, Fabrication Branch

FOR THE DIRECTOR



PETER A. VAN SPILINTER  
Director, Technical Operations Division

AD-A162436

## REPORT DOCUMENTATION PAGE

1a. REPORT SECURITY CLASSIFICATION <b>UNCLASSIFIED</b>		1b. RESTRICTIVE MARKINGS	
2a. SECURITY CLASSIFICATION AUTHORITY		3. DISTRIBUTION/AVAILABILITY OF REPORT Approved for Public Release, Distribution is Unlimited.	
2b. DECLASSIFICATION/DOWNGRADING SCHEDULE		5. MONITORING ORGANIZATION REPORT NUMBER(S)	
4. PERFORMING ORGANIZATION REPORT NUMBER(S)  <b>AFRPL-TR-85-076</b>		7a. NAME OF MONITORING ORGANIZATION	
6a. NAME OF PERFORMING ORGANIZATION  <b>Air Force Rocket Propulsion Lab. TOF</b>	5b. OFFICE SYMBOL (If applicable)	7b. ADDRESS (City, State and ZIP Code)	
6c. ADDRESS (City, State and ZIP Code) <b>AFRPL/TOF, Stop 24 Edwards Air Force Base, CA 93523-5000</b>		9. PROCUREMENT INSTRUMENT IDENTIFICATION NUMBER	
8a. NAME OF FUNDING/SPONSORING ORGANIZATION	8b. OFFICE SYMBOL (If applicable)	10. SOURCE OF FUNDING NOS.	
8c. ADDRESS (City, State and ZIP Code)		PROGRAM ELEMENT NO <b>62302F</b>	PROJECT NO. <b>9983</b>
11. TITLE (Include Security Classification) <b>A DIFFUSER HEAT TRANSFER AND EROSION CODE (U)</b>		TASK NO. <b>FV</b>	WORK UNIT NO. <b>YC</b>
12. PERSONAL AUTHOR(S) <b>Buzzard, Gale H.</b>			
13a. TYPE OF REPORT <b>Final</b>	13b. TIME COVERED FROM <b>83/10</b> TO <b>85/07</b>	14. DATE OF REPORT (Yr., Mo., Day) <b>85/10</b>	15. PAGE COUNT
16. SUPPLEMENTARY NOTATION <b>Gale H. Buzzard is an assistant professor of Mechanical Engineering at Duke University in Durham, North Carolina.</b>			
17. COSAT CODES		18. SUBJECT TERMS (Continue on reverse if necessary and identify by block number)	
SERIAL	GROUP	SUB GR.	
21	08	Diffuser Heat Transfer; Erosion Analysis; Two Phase Flows; Particle Impaction; Ground Test Facilities. ←	
21	08	2	
19. ABSTRACT (Continue on reverse if necessary and identify by block number) A computer code for diffuser heat transfer and erosion analysis (DHTE) has been developed which improves upon the earlier Rocket Engine Diffuser Thermal Analysis Program (REDTAP) of <del>Frout and McCay</del> . Improvements contained within DHTE include provision for a radial temperature gradient within the diffuser wall, an improved model for the particle impingement accommodation coefficient, a model for particle debris shielding, and a model for wall erosion by particle impact. DHTE differs from an earlier diffuser heat transfer code (DHT) to the extent that it incorporates a simple erosion model and utilizes a more recent diffuser version of the JANNAF Standardized Plume Flow Field Model (SCP2ND).  The 77-inch diffuser located at the Air Force Rocket Propulsion Laboratory was instrumented to record the water side wall temperature and water jacket temperature at selected sites along the initial seven feet of the diffuser during routine test firings. Data is presented that supports the predictions of DHTE but is inadequate to validate the code.			
20. DISTRIBUTION/AVAILABILITY OF ABSTRACT <b>UNCLASSIFIED UNLIMITED</b> <input checked="" type="checkbox"/> SAME AS RPT <input type="checkbox"/> DTIC USERS <input type="checkbox"/>		21. ABSTRACT SECURITY CLASSIFICATION <b>UNCLASSIFIED</b>	
22a. NAME OF RESPONSIBLE INDIVIDUAL <b>Richard H. Mickel</b>		22b. TELEPHONE NUMBER (Include Area Code) <b>(805) 277-5434</b>	22c. OFFICE SYMBOL <b>TOF</b>

# TABLE OF CONTENTS

<u>Section</u>		<u>Page</u>
1.	INTRODUCTION	1
2.	STATEMENT OF THE PROBLEM	2
	2.1 General	2
	2.2 Particle Impingement	4
	2.3 Particle Radiation	6
	2.4 Gas Side Convection	7
	2.5 Debris Layer Shielding	8
	2.6 Water Side Convection	12
	2.7 Diffuser Wall Erosion	12
3.	NUMERICAL ANALYSIS	14
4.	IMPLEMENTATION OF DHTE	17
5.	OUTPUT DATA FILES	19
6.	INPUT INFORMATION	20
	6.1 Nomenclature	20
	6.2 Input Procedures	22
	6.3 Input Guidelines	24
7.	OUTPUT INFORMATION	25
	7.1 Nomenclature	25
	7.2 General Description	26
8.	SAMPLE PROBLEM	27
	8.1 General	27
	8.2 Preliminary Calculations	27
	8.3 Input Data	28
	8.4 Execution of Supporting Codes	30
	8.5 Execution of DHTE	32
9.	RESULTS	34
10.	RECOMMENDATIONS	37/38
	REFERENCES	49

Accession For	
NTIS CRA&I	<input checked="" type="checkbox"/>
DTIC TAB	<input type="checkbox"/>
Unannounced	<input type="checkbox"/>
Justification .....	
By .....	
Distribution /	
Availability Codes	
Dist	Avail and/or Special
A-1	



# LIST OF FIGURES

<u>Figure</u>		<u>Page</u>
1	77-Inch Diffuser, AFRPL Area 1-42	39
2	Debris Layer Model	39
3	Finite Difference Grid System	40
4	Axial Temperature Distribution	41
5	Water Side Wall Temperature as a Function of Axial Position, Super BATES, 3 December 1982	42
6	Water Side Wall Temperature as a Function of Time, Super BATES, 3 December 1982	43
7	Water Side Wall Temperature as a Function of Time, Super BATES, 3 December 1982	44
8	Water Side Wall Temperature as a Function of Axial Position, Super BATES, 13 January 1983	45
9	Water Side Wall Temperature as a Function of Time, Super BATES, 13 January 1983	46
10	Water Side Wall Temperature as a Function of Axial Position, Super BATES, 8 November 1983	47
11	Water Side Wall Temperature as a Function of Time, Super BATES, 8 November 1983	48

## 1. INTRODUCTION

A computer program has been developed that performs a thermal analysis of a water jacketed rocket motor test diffuser, and includes a prediction of the erosion rate resulting from particle impingement. The program has been developed to handle the requirements of the particle laden plume associated with a metallized solid propellant, but is also capable of handling a particle free plume. The program combines the earlier work of Trout and McCay<sup>1</sup>, Pergament<sup>2</sup>, and Kessel<sup>3</sup>. The end result is a Diffuser Heat Transfer and Erosion code (DHTE) which corrects several of the shortcomings of the Rocket Engine Thermal Analysis Program (REDTAP) created by Trout and McCay, and includes several areas not treated by the earlier code. Included among these areas are radial temperature gradient within the diffuser wall, an improved model for the particle impingement accommodation coefficient, particle debris shielding, and erosion. DHTE is a modification of a Diffuser Heat Transfer code (DHT) developed by Buzzard<sup>4</sup> and differs from DHT to the extent that it incorporates the simplistic erosion model suggested by Jordan, Girata, Simmons, Sherrel, and McGregor<sup>5</sup>, and utilizes a more recent version of the diffuser flow field model which does not suffer from the problems cited in the description of DHT.

In conjunction with the development of the DHT code, the 77-inch diffuser located at the Air Force Rocket Propulsion Laboratory (AFRPL) Area 1-42 was instrumented to record water side wall temperature at selected sites along the initial seven feet of the diffuser during routine test firings. It was anticipated that data would be available on time to validate the predictions of the model. Unfortunately, the test firings to date continue to involve motors that are too small and/or burn times that are too short to provide useful data. The apparent quality of the data thus far has been excellent, and there remains the promise of useful data in the future. However, much remains to be done in terms of validating the predictions of DHTE.

As was the case with the earlier codes, DHTE relies on the AFRPL Solid Performance Program (SPP)<sup>6</sup> and a diffuser version of the Joint Army Navy NASA Air Force (JANNAF) Standardized Plume Flow Field Model (SCP2ND)<sup>7</sup> to provide the flow field data within the diffuser. SCP2ND has, however, exhibited none of the problems associated with the earlier version (SCIPPY) and includes an automated interface for use with either Version 4 or Version 5 of SPP. DHTE

incorporates the Inter-Agency Chemical Rocket Propulsion Group Turbulent Boundary Layer code (TBL)<sup>8</sup> as a subroutine to handle the gas side convective heat transfer.

## 2. STATEMENT OF THE PROBLEM

### 2.1 General

The computer code developed, and all discussions that follow, deal specifically with the 77-inch diffuser located at AFRPL Area 1-42. The code, however, is written to perform a thermal analysis for any similar diffuser and could be easily modified to handle most water jacketed configurations.

Figure 1 is a schematic of the diffuser which has a uniform diameter inlet section followed by a conical transition to a second uniform diameter section and conical expansion. This final expansion connects to a plenum which removes the rocket motor exhaust gases and maintains the reduced pressure necessary to simulate altitude conditions.

The diffuser is fabricated from ASME-SA-285-C steel, and has a 0.50-inch inner wall which forms the containment for the exhaust plume. The water jacket is formed by this and a 0.375-inch outer wall. These two walls are separated by 2.5 x 2.5 x 0.5-inch angle wound with a 5.75-inch pitch quadruple lead that results in four parallel coolant passages approximately 5.25 x 2.75 inches. These angle members are welded to the inner wall. No attempt has been made to analyze the thermal path added by these angle members. One can assume that they will provide additional cooling of the inner wall but the extent of this effect is indeterminate. There is the added complication of a nominal 0.25-inch radial clearance between the inner assembly and the outer wall. Since the inner assembly floats within the outer wall, the resulting radial clearance can range from 0 to 0.50 inch. It is assumed that this condition does not short circuit the helical path of the water jacket. This is a question that must be addressed as experimental data becomes available.

The heat load on the diffuser is comprised of the convective load from the exhaust gases plus the various particle related heat fluxes. The particles carry with them a very significant quantity of thermal energy as a result of their heat capacity and elevated temperature as compared with the gas side wall temperature of the diffuser. They also carry a very significant

quantity of kinetic energy. If, as they impact the wall, an appreciable portion of either of these energies is transferred to the diffuser wall, a very severe heat load will result. Crucial to a valid diffuser model is the selection or development of a particle impingement model that adequately handles the exchange of these two forms of energy. Radiant exchange from the particles to the wall is a nonnegligible, but distinctly second order, heat load.

The diffuser wall must obey the unsteady heat equation. It is convenient to note that the wall is thin compared with the diffuser radius and to write the heat equation in two-dimensional Cartesian coordinates. As such, the wall temperature is governed by

$$\frac{\partial^2 T}{\partial x^2} + \frac{\partial^2 T}{\partial y^2} = (\rho C/k) \partial T / \partial t \quad (1)$$

where  $x$  and  $y$  are measured parallel and normal to the diffuser wall and  $\rho$ ,  $C$  and  $k$  are the density, specific heat and thermal conductivity of the diffuser wall.

The fluid flow within the water jacket is assumed to be one-dimensional constant property steady flow. It is assumed that the flow rate is known and, therefore, the local fluid velocity is a simple function of the local water jacket cross-sectional area. The temperature distribution within the water jacket is assumed to be a one-dimensional axial transient superimposed upon the steady flow and involving negligible axial conduction. As such, the water jacket temperature is governed by

$$U \frac{\partial T}{\partial x} + (2\pi R h / \rho C A) (T - T_{\text{wall}}) = -\partial T / \partial t \quad (2)$$

where  $U$  is the axial velocity of the coolant,  $R$  is the outer radius of the inner wall,  $\rho$  and  $C$  are the density and specific heat of the coolant,  $A$  is a axial cross-sectional area of the water jacket, and  $h$  is the water side film coefficient. The outer wall of the water jacket is treated as an adiabatic surface. Equations 1 and 2 are solved using explicit finite difference techniques.



## 2.2 Particle Impingement

The aluminum oxide particles contained within the exhaust of a metallized solid rocket motor carry with them a considerable quantity of thermal and kinetic energy. It is convenient to measure the thermal energy relative to the diffuser gas side wall temperature, and to partition the kinetic energy into a component resulting from the velocity parallel to the diffuser wall and a component resulting from the velocity normal to the wall. In this form the potential heat load caused by the particles impinging on the diffuser wall may be represented by

$$\dot{m}_p C_p (T_p - T_w) + \dot{m}_p U_p^2 / 2 + \dot{m}_p V_p^2 / 2$$

where  $\dot{m}_p$  is the mass flow of particles impinging upon the wall,  $C_p$  is the specific heat of the particles,  $T_p$  is the temperature of the particle,  $T_w$  is the diffuser gas side wall temperature,  $U_p$  is the velocity of the particle parallel to the wall and  $V_p$  is the velocity of the particle normal to the wall.

It is common practice to quantify the particle/wall interaction in terms of three accommodation coefficients ( $C_T$ ,  $C_U$  and  $C_V$ ) which define the fraction of each energy component that is transferred to the diffuser wall. Introducing this concept, the heat load on the diffuser wall due to particle impingement is given by the following expression

$$q_{imp} = \dot{m}_p \left[ C_T C_p (T_p - T_w) + C_U U_p^2 / 2 + C_V V_p^2 / 2 \right] \quad (3)$$

Evaluation of these accommodation coefficients is in large measure a question of particle behavior upon impact with the wall. If the particles adhere to the wall, all three accommodation coefficients are unity, and the impingement heat flux will be the dominant heat load on the diffuser. Such an assumption would be a very safe estimate of the maximum heat flux but, if overly conservative, would preclude the testing of rocket motors that could, in reality, be safely tested within the facility. Particle impingement with the wall can be expected to occur at a relatively shallow angle. This lends credence to an assumption that the particles do not adhere to the wall and that the thermal accommodation coefficient is close to zero. A further

consequence of this assumption would be that the momentum of the particle parallel to the surface, and therefore that component of the kinetic energy, will be conserved. This would lead to a  $C_y$  equal to zero. Visual inspection following two Super BATES firings revealed no evidence of significant particle deposition on the diffuser wall.

The transfer of the component of kinetic energy normal to the surface from the particle to the surface can be related to the coefficient of restitution for the collision. After a review of the limited data available, Kessel<sup>3</sup> suggests the use of a coefficient of restitution equal to  $(1 - B/90)$ , where  $B$  is the angle of impact, as measured in degrees, between the velocity vector and the normal to the surface. This leads to the following expressions where  $V_p$  is the component of the velocity normal to the surface and the prime denotes conditions following impact.

$$V'_p/V_p = 1 - B/90$$

$$(KE'/KE)_{\text{normal}} = (1 - B/90)^2$$

$$(\Delta KE/KE)_{\text{normal}} = (B/90)(2 - B/90)$$

The decrease in the normal component of kinetic energy places an upper boundary on the energy transferred to the surface. Unless the particle adheres to the surface, a portion of this energy will be carried away as an increase in the internal energy of the particle. Citing limited data that support an accommodation coefficient of 0.55 to 0.70 for normal impact and noting that the quantity

$$(B/90)(2 - B/90)$$

is approximated within  $\pm 7\%$  by  $1.15 \sin B$  for  $B$  less than or equal to 40 degrees, Kessel suggests the use of an accommodation coefficient

$$C_y = 0.8 \sin B \tag{4}$$

The heat load associated with particle impingement is handled within DHTE as per Equation 3, with the user allowed to specify any desired set values for

the accommodation coefficients. SCP2ND will provide DHTE with local values for the angle  $B$ , and an option is provided that allows the use of Equation 4 along with the ability to scale the coefficient of  $\sin B$  up or down at will. In reporting on data gathered at Arnold Engineering Development Center (AEDC) on an instrumented diffuser, Kessel<sup>3</sup> cites modest agreement between the experimental data and the predictions of REDTAP using accommodation coefficients of 0, 0, and  $0.8 \sin B$  along with a specified average value of  $B$  equal to 22 degrees. Experimental data to be presented later in this report shows relatively good agreement with the predictions of DHTE using a  $C_T$  of 0.25,  $C_U$  of 0, and  $C_V$  of  $0.8 \sin B$ .

### 2.3 Particle Radiation

No attempt is made in the present work to alter the radiation model developed within REDTAP by Trout and McCay. This is a very simplistic model that places a believable upper limit on the contribution of particle radiation to the heat load on the diffuser. All particle properties at the rocket motor exit plane are generated by or dependent upon information generated by SPP. Version 4 of SPP provides three particle size groups with a very limited amount of size control in the user's hands. Considerable controversy surrounds actual particle size distribution and whether or not the three size groups generated by SPP result in an adequate particle flow field within the nozzle and diffuser. Any shortcomings of SPP in this area are passed on to SCP2ND. Presumably, Version 5 of SPP will give the user considerably more control over the particle size. The radiation heat load is a minor threat to the diffuser, and until the particle flow field is better defined, a more refined model does not seem justified.

It is assumed that the flow field is optically thin and that the particles behave as gray bodies emitting radiation as per the Stefan-Boltzman equation with all the properties evaluated in terms of centerline conditions at the rocket motor exit plane. It is further assumed that this emissive power is concentrated as a line source of uniform strength along the diffuser centerline. This source strength is readily evaluated in terms of exit plane information from SPP or SCP2ND and takes the form

$$q = 3 \dot{m}_p \epsilon \sigma T_p^4 / U_p \rho_p R_p \quad (5)$$

where  $\sigma$  is the Stefan-Boltzman constant and  $\dot{m}_p$  is the mass flow rate,  $\epsilon$  the emissivity,  $T_p$  the temperature,  $U_p$  the axial velocity,  $\rho_p$  the mass density, and  $R_p$  the particle radius associated with the particle group in question. Equation 5 must be summed over the particle groups present. Defense of this model as used in REDTAP was supported by the assumption of a thermal accommodation coefficient of unity. This resulted in a particle impingement heat load so large as to render the radiation load negligible. With the accommodation coefficients suggested by the present study, the radiation load will become a significant, but not major, portion of the diffuser heat load. On the other hand, the present assumption that the particles do not adhere to the wall lends some credence to the assumption of a uniform strength line source of radiation. As a body of experimental data becomes available and SCP2ND run in conjunction with Version 5 of SPP provides more reliable predictions of the particle flow field, a refinement of this model should be considered.

#### 2.4 Gas Side Convection

The gas side convection heat transfer is handled within DHTE by incorporating TBL as a subroutine in much the same fashion as was done in REDTAP. SCP2ND provides TBL with the edge conditions for the boundary layer analysis, and TBL provides DHTE with the film coefficients and adiabatic wall temperatures required for the heat transfer calculation. The boundary layer grows from a stagnation region at the point of plume impingement and therefore it is necessary to start the boundary layer with nonzero initial values for the momentum and energy thicknesses. REDTAP started TBL with these two parameters set equal to a single arbitrarily small number. DHT attempted to approximate the impingement point heat transfer and set the initial values of the boundary layer thicknesses equal to values that would cause TBL to match this initial heat transfer rate. This approach had merit but was admittedly arbitrary. SCP2ND is accompanied with a Diffuser Wall Boundary Layer Initialization code (DWBLI) which solves for the flow field in the region of impingement and outputs initial values for the boundary layer thicknesses. DHTE utilizes DWBLI for the initial boundary layer thicknesses. When compared

with preliminary experimental data from three Super BATES firings, these initial conditions result in DHTE predictions that consistently overpredict the impingement point heat transfer but compare well further downstream.

## 2.5 Debris Layer Shielding

The assumption that the particles which strike the wall do not adhere to the wall gives rise to an accumulation of these particles in the vicinity of the wall. As this accumulation is swept downstream by the main flow, it will form an increasingly dense sheath of particles adjacent to the wall and will partially shield the wall from particle impingement. Wickman, Mockenhaupt, and Ditore<sup>9</sup> developed a simple model for this phenomenon and present supporting data in conjunction for an erosion study. The essentials of their model are contained in Figure 2. The model assumes a single particle size and a cross-sectional area for collision equal to  $\sigma$ . Assuming a particle number density  $n$ , within the debris layer, the cross-sectional area blocked per unit area by the debris is found to be

$$n \sigma dx / \sin B.$$

Assuming an incident particle flow with a particle number density  $N$ , the change in particle number density caused by scattering within the debris layer element  $dx$  will be

$$dN = -N n \sigma dx / \sin B.$$

Collecting like terms and integrating across the debris layer

$$\ln(N_w/N_o) = - \sigma \int_0^d n dx / \sin B \quad (6)$$

where  $N_w$  is the incident particle number density at the wall,  $N_o$  is the incident particle number density at the outer edge of the debris layer, and their ratio represents the fraction of the incident particles reaching the wall. While neither  $n$  nor  $d$  is known, the above integral is related to the local mass flow rate of debris through

$$\dot{m}_d = \int_0^d 2\pi R m_p U_d dx$$

where  $R$  is the local diffuser radius,  $m_p$  is the particle mass, and  $U_d$  is the velocity of the debris. Assuming that the debris is swept along by the edge velocity of the gas,  $U_g$ , one can replace  $U_d$  with  $U_g$  and solve for the integral contained in the above expression as

$$\int_0^d n dx = \dot{m}_d / 2\pi R m_p U_g.$$

Substituting this expression into Equation 6 one obtains

$$\ln(N_w/N_o) = -\sigma \dot{m}_d / 2\pi R m_p U_g \sin B \quad (7)$$

In the case of diffuser flow,  $\dot{m}_p$  is obtained by summing the particle mass flux impinging upstream of the point in question. Information necessary for evaluating everything except  $\sigma$  is available from SCP2ND.

The model just described is readily expanded to include flows involving more than a single size particle. It is convenient to treat each particle size group individually. Assuming three size groups with group  $j$  assumed to be the incident particle group and group  $k$  the particle debris group, one can consider  $\sigma_{jk}$  as the cross section for particle group  $j$  colliding with particle group  $k$ ,  $N_j$  the particle number density of the impinging particles, and  $n_k$  the particle number density of the debris. With this nomenclature, Equation 6 may be written as

$$\ln(N_w/N_o)_j = -\sum_{k=1}^3 \sigma_{jk} \int_0^H n_k dx / \sin B_j \quad (8)$$

where  $H$  is sufficiently large to include all three debris layers. The right hand side of Equation 8 may be expanded and, noting that as  $x$  extends to  $d$ ,  $n$  tends to zero, the upper limit of each integral may be replaced with the individual debris layer thickness, leading to the following form:

$$\ln(N_w/N_o)_j = -\sum_{k=1}^3 \sigma_{jk} \int_0^{d_k} n_k dx / \sin B_j. \quad (9)$$

As with Equation 7, it is convenient to recognize that

$$\int_0^d n_k dx = \dot{m}_k / 2\pi R m_k U_g$$

where  $\dot{m}_k$  is the mass flow rate of particle group  $k$  within the debris layer and  $m_k$  is the mass of a group  $k$  particle. Introducing this into Equation 9 leads to

$$\ln(N_w/N_o)_j = -\sum_{k=1}^3 (\sigma_{jk} \dot{m}_k / m_k) / 2\pi R U_g \sin B_j.$$

Noting that, with the exception of  $\sin B_j$ , the above expression is solely a function of the debris layer, it is convenient to define DF, the debris factor, such that

$$\ln(DF_j) = -\sum_{k=1}^3 (\sigma_{jk} \dot{m}_k / m_k) / 2\pi R U_g \quad (10A)$$

and

$$(N_w/N_o)_j = (DF_j)^{1/\sin B_j} \quad (10B)$$

No mention has been made thus far as to evaluating  $\sigma_{jk}$ . In the development of their particle diameter model, Wickman, et al, assume that any contact at all between impinging particle and debris particle will result in the scattering of the impinging particle. This model leads to

$$\sigma = \pi(2R_p)^2$$

which would appear to be excessive. The model built into DHTE assumes that a smaller particle will be scattered by as little as grazing contact, that an equal size particle will require an angle of impact of at least 45 degrees, and that a larger particle must impact a smaller particle with an angle of at least 45 degrees and impact an aggregate mass of such particles equal to its own mass before scattering will occur. This leads to

$$\sigma_{jk} = \begin{cases} \pi(R_j + R_k)^2 & R_j < R_k \\ \pi(R_j + R_k)^2 (R_k/R_j)^{3/2} & R_j \geq R_k \end{cases}$$

introducing this model for  $\pi_{jk}$  and noting that

$$\dot{m}_k = 4\pi R_k^3 \rho_p / 3$$

one is able to evaluate the individual terms of the right hand side of Equation 10A as

$$\sigma_{jk} \dot{m}_k / 2\pi R U_g \dot{m}_k = \begin{cases} 3(R_j + R_k)^2 \dot{m}_k / 8\pi R U_g \rho_p R_k^3 & R_j < R_k \\ 3(R_j + R_k)^2 \dot{m}_k / 16\pi R U_g \rho_p R_j^3 & R_j \geq R_k \end{cases} \quad (11)$$

The above debris shielding model has been built into DHTE and the user is provided with the option to use or not use it in the calculations. If the option is implemented, the particle mass flow rate that appears in Equation 3 will be multiplied by the factor

$$(DF_j)^{1/\sin B_j}$$

For the examples looked at to date, debris shielding has not appeared to be a significant factor. The debris factor has ranged from 1.0 to 0.9, but has remained very close to 1.0 in the regions where impingement heating was a major concern. This is understandable since only after particles impinge upon the wall for some distance does the debris layer build up to an effective shield. The reduction of particle mass flux reaching the wall may be as great as 50% in some regions, but these regions are well downstream of the severe heat load areas. The regions where appreciable debris shielding occurs are where the impingement angle is quite shallow and

$$(DF_j)^{1/\sin b_j}$$

can become quite small.



## 2.6 Water Side Convection

The water side film coefficient is evaluated using correlations presented by Marks.<sup>10</sup> The preliminary calculation is handled by

$$h' = 160 (1 + 0.012 T_f) v^{0.8} / D_h^{0.2} \quad (12)$$

where  $T_f$  is the film temperature of the water measured in degrees Fahrenheit,  $v$  is the velocity of the water measured in feet per second,  $D_h$  is the hydraulic diameter ( $4 \times \text{area} / \text{perimeter}$ ) of the channel measured in inches, and  $h'$  is the film coefficient measured in B/hr-ft<sup>2</sup>-F. This value for  $h$  is modified to compensate for the radius of curvature of the channel ( $D_c/2$ ) such that

$$h = (1 + 3.5 (D_h/D_c)) h'. \quad (13)$$

## 2.7 Diffuser Wall Erosion

Jordan, et al<sup>5</sup>, cite diffuser wall erosion rates as high as 0.001 in/sec and protective liner erosion rates as high as 0.065 in/sec in conjunction with tests of the M-X Stage II engine in the AEDC J-4 test cell. Based upon this data, erosion may be as severe a threat or possibly a greater threat to diffuser survivability than is thermal damage. They suggest that erosion may be modeled on the basis of the particles mass loss ratio,  $G$ , where

$$G = \frac{\text{mass flux lost from the wall}}{\text{mass flux of particles impinging upon the wall}}$$

Whereas the mass loss ratio is a strong function of the physical properties of the wall and the particles, they note that for a given facility and assuming similar particles,  $G$  should model as per particle kinetic energy. Based upon this assumption, the ratio of  $G$  to the square of the particle velocity normal to the wall,  $V_p$ , should be a constant for a given test facility. Therefore,

$$G = (G/V_p^2)_{\text{ref}} \times V_p^2$$

$$\dot{m}_{\text{wall}} = (G/V_p^2)_{\text{ref}} \times \dot{m}_p V_p^2$$

and with  $\dot{m}$  measured as (mass/unit area/unit time) the erosion rate  $\dot{s}$  (length/unit time) may be modeled as

$$\dot{s} = (G/V_p^2)_{\text{ref}} \times \dot{m}_p V_p^2 / \dot{m}_{\text{wall}}$$

or for any given facility

$$\dot{s} = K_e \dot{m}_p V_p \quad (14)$$

Jordan, et al<sup>5</sup>, cite the following data for the J-5 test cell at AEDC:

$$V = 9016 \text{ fps @ } 19.2 \text{ deg}$$

$$V_p = 9016 \times \sin 19.2 = 2965 \text{ fps}$$

$$G = 0.0331 \quad (\text{diffuser wall})$$

$$\dot{s} = 0.000385 \text{ in/sec} \quad (\text{diffuser wall})$$

$$\dot{s} = 0.017 \text{ in/sec} \quad (\text{diffuser liner})$$

Based upon assumed densities of the steel wall (490 lb<sub>m</sub>/ft<sup>3</sup>) and the liner (107 lb<sub>m</sub>/ft<sup>3</sup>), the erosion constants for the J-5 cell may be calculated as

$$K_e = 7.68 \times 10^{-12} \text{ ft-sec}^2/\text{lb}_m \quad (\text{diffuser wall})$$

$$K_e = 3.39 \times 10^{-10} \text{ ft-sec}^2/\text{lb}_m \quad (\text{diffuser liner})$$

The above model has been built into DHTE and the erosion rate is calculated locally along the diffuser using Equation 14. There is no reason to expect the erosion constants that have been generated from the AEDC data to apply directly to the AFRPL diffuser. They are starting point estimates and should be adjusted as local erosion rate data become available.

### 3. NUMERICAL ANALYSIS

Figure 3 shows the finite difference grid that is used in solving for the temperature distribution within the diffuser wall and the water jacket.

Equation 1 is formulated in explicit form using central difference approximations for the spatial derivatives and a forward difference approximation for the temporal derivative. This gives rise to

$$\begin{aligned} & (T_{m-1,n} - 2 T_{m,n} + T_{m+1,n})/(\Delta x)^2 \\ & + (T_{m,n-1} - 2 T_{m,n} + T_{m,n+1})/(\Delta y)^2 \\ & = (\rho C/k)(T_{m,n}^+ - T_{m,n}) / \Delta t \end{aligned} \quad (15)$$

where the superscript + indicates a temperature occurring at time  $(t + \Delta t)$ . Equation 15 may be solved for  $T_{m,n}^+$  and written as

$$\begin{aligned} T_{m,n}^+ &= (T_{m,n-1} + T_{m,n+1} + Z^2(T_{m-1,n} + T_{m+1,n}) \\ &+ (M1 - 2 - 2 Z^2) T_{m,n}) / M1 \end{aligned} \quad (16)$$

where

$$Z = (\Delta y / \Delta x) \cos \phi$$

and

$$M1 = \rho C (\Delta y)^2 / k \Delta t.$$

In this form the temperature distribution at time  $(t + \Delta t)$  may be solved for point by point in terms of a known temperature distribution at time  $t$ . This explicit formulation has the stability requirement that

$$M1 - 2 - 2 Z^2 \geq 0$$

For a given  $\Delta X$  and  $\Delta Y$  this places an upper bound on  $\Delta t$  but has presented no problems to date.

Equation 16 is applicable to all internal nodes. However, the first radial node  $(m,1)$  and the last radial node  $(m,L)$  involve boundary conditions and must be handled separately. In the case of these two nodes, it is convenient to forsake the mathematical elegance of finite difference forms and to perform an energy balance on the element. Note that in terms of thermal capacity each of these nodes involves only one half an element. Written in explicit form for node  $m,1$  this takes on the following form:

$$\begin{aligned}
 & h_m \Delta X (T_{AW_m} - T_{m,1}) + (k \Delta Y / 2 \Delta X) (T_{m-1,1} - T_{m,1}) \\
 & + (k \Delta Y / 2 \Delta X) (T_{m+1,1} - T_{m,1}) + (k \Delta X / \Delta Y) (T_{m,2} - T_{m,1}) \\
 & + QPR_m \Delta X (T_p - T_{m,1}) + QPI_m \Delta X + QPR_m \Delta X \\
 & = (\rho C \Delta X \Delta Y / 2 \Delta t) (T_{m,1}^+ - T_{m,1})
 \end{aligned} \tag{17}$$

where  $h$  is the gas side film coefficient,  $T_{AW}$  is the adiabatic wall temperature of the gas,  $QPT$  is the thermal energy flux per unit area caused by particle impingement,  $QPI$  is the inertial energy flux per unit area caused by particle impingement, and  $QPR$  is the radiant energy flux per unit area from the particles. Equation 17 may be solved for  $T_{m,1}^+$  and written as

$$\begin{aligned}
 T_{m,1}^+ &= (2T_{m,2} + Z^2(T_{m-1,1} + T_{m+1,1}) + 2N1 T_{AW_m} \\
 & + (2QPT_m \Delta Y / k) T_p + (2 \Delta Y / k) (QPI_m + QPR_m) \\
 & + (M1 - 2 - 2Z^2 - 2N1 - 2QPT_m \Delta Y / k) T_{m,1}) / M1
 \end{aligned} \tag{18}$$

where

$$N1 = h \Delta Y / k.$$

Here as with Equation 16, one has the simplicity of an explicit formulation, but the stability restriction that

$$M1 - 2 - 2Z^2 - 2N1 - 2QPT_m \Delta Y / k \geq 0$$

which places a slightly smaller upper limit on  $\Delta t$  than was associated with Equation 16.

Node  $m, L$  may be handled in the same fashion as node  $m, 1$  and results in

$$T_{m,L}^+ = (2T_{m,L-1} + Z^2(T_{m-1,L} + T_{m+1,L}) + 2N2 TC_m) \quad (19)$$

$$+ (M1 - 2 - 2Z^2 - 2N2) T_{m,L} / M1$$

where  $TC$  is the local coolant temperature and  $N2$  is identical to  $N1$  only based upon the water side film coefficient. In this case stability requires that

$$M1 - 2 - 2Z^2 - 2N2 \geq 0$$

which places an additional upper bound on  $\Delta t$ .

An attempt to handle Equation 2 in the same fashion as Equation 1, that is to say, using a central difference approximation for the spatial derivative and a forward difference approximation for the temporal derivative will lead to numerical instability. On the other hand, using a backward difference approximation for the spatial derivative will lead to a stable formulation. Using this latter approach, Equation 2 may be approximated by

$$\begin{aligned} & U_m (TC_m - TC_{m-1}) / \Delta X + (2\pi R_m h_m / \rho C A_m) (TC_m - T_{m,L}) \\ & = - (TC_m^+ - TC_m) / \Delta t \end{aligned}$$

Solving for  $TC_m^+$

$$TC_m^+ = [TC_{m-1} + N3 T_{m,L} + (M2 - 1 - N3) TC_m] / M2 \quad (20)$$

where

$$M2 = \Delta X / U_m \Delta t = A_m \Delta X / \dot{m} \Delta t \cos \phi$$

and

$$N3 = 2\pi R_m h_m \Delta X / \dot{m} C \cos \theta$$

and  $\dot{m}$  is the mass flow rate of the coolant. Stability will require that

$$M2 - 1 - N3 \geq 0$$

and place yet another upper bound on  $\Delta t$ .

#### 4. IMPLEMENTATION OF DHTE

The following discussion is intended to be an overview of the code. Detailed discussion of the input and output will appear separately.

Prior to executing DHTE, SPP must be run for the rocket motor and SCP2ND must be run for the diffuser. It is assumed that the user will consult the users guides provided with these codes; however, a limited commentary will be included in conjunction with the sample problem presented later in the report. SPFI, SCP2ND, and DWBLI are all three described within the users guide for SCP2ND<sup>7</sup>. SPFI provides the interface between SPP and SCP2ND. All that is required by SPFI, in addition to the output generated by SPP, is a small input file on diffuser data. SPFI will generate an output on TAPE1 that must be cataloged for use as an input for SCP2ND. While SPP solves for the flow field within the entire rocket motor nozzle, SCP2ND will perform its own solution of the nozzle's supersonic portion prior to solving for the flow field within the diffuser. For this reason, SCP2ND will save sufficient information to allow a user to change parameters within the diffuser and restart the diffuser solution without repeating the nozzle solution. This information is stored as SCFILE and should be cataloged for future use. SCP2ND will store information for use by DWBLI in a file named AEDCINV, and will store the boundary layer edge conditions needed by DHTE as TAPE99. These two files will need to be cataloged for use by DWBLI and DHTE. DWBLI will generate the initial values of momentum thickness and energy thickness needed by TBL for use within DHTE.

The units for input data are selected on the basis of user convenience and are converted internally to pounds force, feet, seconds, degrees Rankine, and pounds mass. The units for output are selected on the basis of user convenience.

The edge condition data provided by SCP2ND on TAPE99 are randomly spaced along the diffuser axis. Since the numerical analysis within DHTE assumes a uniformly spaced grid system, the first major operation within DHTE is to read the SCP2ND tape and to interpolate within the data to create a set of uniformly spaced edge conditions. In conjunction with this manipulation, all edge condition type calculations within the DHTE model are also performed. These include the calculation of the particle impingement mass flux, debris layer data, erosion rates, and particle related heat fluxes. In as much as neither the rocket motor chamber pressure nor the test cell pressure remain constant throughout the test, provision is made to update the edge conditions by way of additional SCP2ND tapes. This provision is handled through the index SCIPPY and numbered data sets identified as SCIP(1) through SCIP(SCIPPY).

Once the edge conditions have been established, DHTE calls TBL to obtain the gas side film coefficients and the adiabatic gas wall temperatures. Since the film coefficients predicted by TBL are mild functions of the gas side surface temperatures, provision is made through the parameter DCALL to update the film coefficients as the diffuser wall temperature rises. The code has an initial update built into it that occurs ten time increments into the calculations. Subsequent to this, an update occurs every DCALL time increments or with each new set of edge conditions obtained from a SCP2ND tape. TBL is a time consuming code and indiscriminate updating should be avoided. To date, it has been adequate to update TBL just prior to the final output and to verify that no significant changes have occurred in the film coefficients.

Many of the coefficients within the governing equations are independent of temperature and are evaluated as a preliminary calculation. Much of this information is output as a matter of user convenience.

The output that occurs at time zero or following the reading of a new SCP2ND tape is quite extensive and contains a great deal of boundary layer, debris layer, erosion, and individual heat flux information that will remain constant throughout the calculations. Future output will occur every DOUT time increments and is appreciably abbreviated.

If the parameter DAFLAG has been read in as other than zero, DHTE has the capability to create output files containing gas side wall temperature, water side wall temperature, and coolant temperature as functions of either time or

position. Unless this option is implemented, temperatures are stored for time  $t$  and  $t + \Delta t$  only. A more extensive discussion of this option is found in Section 5.

The main heat transfer calculation is an implementation of the finite difference equations presented earlier in Section 3. It is appropriate at this time to comment on the handling of the end conditions. The near and far end of the diffuser wall are treated as adiabatic planes. These conditions are implemented by extending the grid system one grid line beyond each end and step by step assigning the outboard nodes mirror image values from internal nodes. This allows nodes located on the two end planes to be handled as though they were internal nodes and introduces no special equations for these nodes. The coolant temperature at the diffuser inlet plane is held at the supply temperature and the upstream differencing used within Equation 20 requires no knowledge of coolant temperature beyond the diffuser exit plane.

Following each time step there is the opportunity to output the temperature distribution through the parameter DOUT, to store a portion of the temperature data under DAFLAG option, to update the gas side film coefficients under the DCALL option, and to update the edge conditions with a new SCP2ND tape. Independent of any of the above mentioned options, the water side film coefficients are functions of the average film temperatures and are updated following each time step.

## 5. OUTPUT DATA FILES

Provision is made for creating and saving data files for future use. This option is implemented by setting DAFLAG equal to any nonzero integer. Data sets will be written to TAPE99.

Temperature is stored as a function of axial position each time that DHTE calls for printed output. Each data set is preceded by a message stating the time in seconds at which it occurred. The data set consists of four columns of data. Column 1 lists axial position in inches on a grid interval of DMXBA. Columns 2, 3, and 4 list the gas side wall temperature, the water side wall temperature, and the coolant temperature at these axial positions. Following the above data sets, temperature is stored as a function of time at as many as five user specified axial grid locations specified by MDATA. Each data set is preceded by a message indicating the axial location in inches. Column 1 lists



time in seconds on a interval of DDAOUT integration steps and columns 2 through 4 list the corresponding gas side and water side wall temperatures and the coolant temperature. As DHTE is currently dimensioned, DDAOUT must be selected such that these data sets contain no more than 100 entries per column. Temperature is stored in degrees Fahrenheit to be consistent with the data handling practices at Area 1-42.

## 6. INPUT INFORMATION

### 6.1 Nomenclature

<u>Variable</u>	<u>Description</u>	<u>Type</u>
ACN	Accommodation coefficient, kinetic energy normal to the diffuser wall (none)	Real
ACP	Accommodation coefficient, kinetic energy parallel to the diffuser wall (none)	Real
ACT	Accommodation coefficient, thermal energy (none)	Real
DAFLAG	Flag. Data sets are stored if DAFLAG is nonzero. (none)	Integer
DCALL	Frequency of TBL update, every DCALL time steps (none)	Integer
DDAOUT	Frequency with which temperature is saved as a function of time under the DAFLAG option, every DDAOUT time steps (As currently dimensioned, NDTAU/DDAOUT may not exceed 99 (none)	Integer
DISCH	Volumetric flow rate of coolant (gpm)	Real
DMXBA	Frequency with which temperature is saved as a function of axial position under the DAFLAG option, every DMXBA grid lines (none)	Integer
DOUT	Frequency of printed output, every DOUT time steps (none)	Integer
DTAU	Time step size (sec)	Real
DX	Axial step size (inches)	Real
DXMAX	Maximum allowable step size within TBL (inches)	Real
ENDTBL(K)	Last time step for which the Kth SCP2ND tape should be used (none)	Integer
EROCL	Erosion constant for the liner ( $\text{ft-sec}^2/\text{lb}_m$ )	Real
EROCW	Erosion constant for the wall ( $\text{ft-sec}^2/\text{lb}_m$ )	Real
GAMO(K)	Stagnation ratio of specific heats associated with the Kth SCP2ND tape (none)	Real

<u>Variable</u>	<u>Description</u>	<u>Type</u>
HT	Radial height of the water jacket passage (inches)	Real
KRPIK(K)	Radiation source strength associated with the Kth SCP2ND tape (B/sec-ft)	Real
KW	Thermal conductivity of the diffuser wall (B/sec-ft-R)	Real
MDATA(N)	Axial grid location at which temperature is to be saved under the DAFLAG option (none)	Integer
MU	Viscosity of the coolant ( $\text{lb}_m/\text{ft-sec}$ )	Real
NCH	Number of coolant channels (none)	Integer
NDATA	Number of axial positions MDATA(N) at which temperature is to be saved under the DAFLAG option (none)	Integer
NDTAU	Number of time steps of numerical integration to be performed (none)	Integer
NDY	Number of diffuser wall elements taken radially (none)	Integer
NSCIP	Number of SCP2ND tapes to be read (none)	Integer
PHIIK(K)	Initial boundary layer momentum thickness associated with the Kth SCP2ND tape (feet)	Real
RBARK	Gas constant associated with the Kth SCP2ND tape ( $\text{ft-lb}/\text{lb}_m\text{-R}$ )	Real
RHOC	Mass density of the coolant ( $\text{lb}_m/\text{ft}^3$ )	Real
RHOW	Mass density of the diffuser wall ( $\text{lb}_m/\text{ft}^3$ )	Real
SCIP(K)	Identifier. Various SCP2ND tapes may be attached as TAPEnn. SCIP(K) is the two digit identifier nn. Provision is made within the DHTE program card for TAPE11 and TAPE12. This may be expanded if the user desires and has the storage space available. (none)	Integer
SPHTC	Specific heat of the coolant ( $\text{B}/\text{lb}_m\text{-R}$ )	Real
SPHTW	Specific heat of the diffuser wall ( $\text{B}/\text{lb}_m\text{-R}$ )	Real
THETAK(K)	Initial boundary layer energy thickness associated with the Kth SCP2ND tape (feet)	Real
TI	Initial temperature (deg R)	Real
TKW	Thickness of the inner wall of the diffuser (inches)	Real
TYPACN	Type ACN TYPACN = 0, ACN = 0.8 ACN SIN B TYPACN $\neq$ 0, ACN = ACN (none)	Integer

<u>Variable</u>	<u>Description</u>	<u>Type</u>
TYPDBR	Type of debris wall analysis TYPDBR = 0, effects of model excluded TYPDBR $\neq$ 0, effects of model included Parameters will be calculated and outputted regardless of the value of TYPDBR (none)	Integer
WIDTH	Width of each coolant channel (inches)	Real
XMOTOR	Distance from the motor exit plane to the diffuser inlet plane. If the motor exit cone extends into the diffuser, XMOTOR will be negative. (inches)	Real
XSTOP	Extent of the diffuser to be analyzed as measured from the diffuser inlet plane (inches)	Real
ZMOUK(K)	Stagnation viscosity associated with the Kth SCP2ND tape (lb <sub>m</sub> /ft-sec)	Real
ZMVISK(K)	Exponent in the viscosity vs temperature model associated with the Kth SCP2ND tape $\text{VISCOSITY} = \text{ZMOUK} (T/T_0)^{\text{ZMVISK}}$ where T <sub>0</sub> is stagnation temperature (none)	Real

## 6.2 Input Procedures

DHTE receives its input in the form of a series of data card images available as TAPE5. Shown below is a card by card description of the format and data contained within each card image.

CARD 1 (12A6)

TITLE FOR THE ANALYSIS

CARD 2 (8F10.4)

DX, DTAU, DXMAX

CARD 3 (8I10)

NDTAU, NDY, NCH, DOUT, DCALL, NSCIP

CARD 4 (8I10)

DAFLAG, DDAOUT, DMXBA, NDATA, MDATA(1), -----, MDATA (NDATA)

If no data sets are to be stored, this card image may be left blank but must be included

CARD 5 (8F10.4)

TKW, WIDTH, HT

CARD 6 (8F10.4)

RHOW, RHOC, SPHTW, SPHTC, KW, MU

CARD 7 (2E10.3)

EROCW, EROCL

CARD 8 (8F10.4)

DISCH, XMOTOR, XSTOP, TI

CARD 9 (8I10)

ACN, ACP, ACT

CARD 10 (8I10)

TYPACN, TYPDBR

CARD 11 (8I10)

SCIP(1), -----, SCIP(NSCIP)

CARD 12 (8I10)

ENDTBL(1), -----, ENDTBL(NSCIP)

CARD 13 (8F10.4)

RBARK(1), -----, RBARK(NSCIP)

CARD 14 (8F10.4)

PRK(1), -----, PRK(NSCIP)

CARD 15 (8F10.4)

ZMOUK(1), -----, ZMOUK(NSCIP)

CARD 16 (8F10.4)

ZMVISK(1), -----, ZMVISK(NSCIP)

CARD 17 (8F10.4)

GAMOK(1), -----, GAMOK(NSCIP)

CARD 18 (8F10.4)

PHI1K(1), -----, PHI1K(NSCIP)

CARD 19 (8F10.4)

THETAK(1), -----, THETAK(NSCIP)

CARD 20 (8F10.4)

KRPIK(1), -----, KRPIK(NSCIP)

### 6.3 Input Guidelines

NSCIP, SCIP(K). For simple analyses, the flow field model within the diffuser will be assumed to remain constant with respect to time, and NSCIP will be set equal to 1. If, on the other hand, either the motor chamber pressure or the test cell pressure change significantly during the burn time, it may be desirable to account for the resulting changes in the diffuser flow field. This may be accomplished by employing two or more SPP and SCP2ND runs and will involve two or more SCP2ND tapes. If the flow conditions were quite similar during the early and late portions of the run, but differed significantly during the middle of the burn time, one could consider using two SCP2ND runs. NSCIP would be read in as 3. The two SCP2ND tapes could be attached as TAPE11 and TAPE12. SCIP(1) would be read in as 11, SCIP(2) would be read in as 12, and SCIP(3) would be read in as 11. ENDTBL(1), ENDTBL(2), and ENDTBL(3) would indicate the last time step for which each set of data would be used. Cards 11 through 20 would contain three entries each. If, as in the example just cited, a given tape is to be used more than one time, there will be duplication among the entries but there will be NSCIP entries per card. Provision has been made in the program card for TAPE11 and TAPE12. The user may expand on this as machine time and space permit. The program is dimensioned to allow NSCIP to be as large as 10.

KRPI(K). See the sample problem for details on calculating this parameter.

## 7. OUTPUT INFORMATION

### 7.1 Nomenclature

<u>Variable</u>	<u>Description</u>
A	Cross-sectional area of the water jacket normal to the diffuser axis ( $\text{ft}^2$ ).
C1	$N1 = C1 \times HG(M) (B/\text{sec-ft}^2-R)^{-1}$ (See Equation 18) $N2 = C1 \times HC(M) (B/\text{sec-ft}^2-R)^{-1}$ (See Equation 19)
DEBRIS(J)	Mass flow rate of the particle group J within the debris layer ( $\text{lb}_m/\text{sec}$ )
DEBRIS FACTOR	That fraction of the incident particle mass flux which reaches the diffuser wall (none) (See Equation 10A)
DELTA	Velocity boundary layer thickness (in)
DP(J)	Particle diameter for group J (microns)
WALL EROSION	Erosion rate for the diffuser wall (in/sec)
LINER EROSION	Erosion rate for the protective liner (in/sec)
HC	Water side heat transfer coefficient ( $B/\text{sec-ft}^2-R$ )
HG	Gas side heat transfer coefficient ( $B/\text{sec-ft}^2-R$ )
KRPIK(K)	Particle radiation source strength associated with the Kth SCP2ND tape ( $B/\text{sec-ft}$ )
M	Axial grid location, M=2 indicates the diffuser inlet (none)
MDOT(J)	Mass flow rate of particle group J impinging upon the wall in the absence of debris layer effects ( $\text{lb}_m/\text{sec-ft}^2$ )
M1	(See Equation 16) (none)
M2	(See Equation 20) (none)
QHC	Water side convective heat flux ( $B/\text{sec-ft}^2$ )
QHG	Gas side convective heat flux ( $B/\text{sec-ft}^2$ )
QPI	Inertial heat flux associated with particle impingement ( $B/\text{sec-ft}^2$ )
QPI(J)	Inertial heat flux associated with particle impingement, group J ( $B/\text{sec-ft}^2$ )

<u>Variable</u>	<u>Description</u>
QPR	Heat flux associated with particle radiation (B/sec-ft <sup>2</sup> )
QPT	Thermal heat flux associated with particle impingement (B/sec-ft <sup>2</sup> )
R	Local diffuser radius (ft)
RE	Reynolds Number for the coolant flow (none)
R1	Local inner radius of the water jacket (ft)
R2	Local outer radius of the water jacket (ft)
SCIPPY	The number of the SCP2ND tape being used (none)
SINE(J)	Sine of the impingement angle with which particle group J strikes the diffuser wall (none)
TAW	Adiabatic wall temperature of the edge condition gas flow (deg R)
V	Coolant velocity (fps)
WALL TEMP	Diffuser wall temperature (deg R)
X	Axial location measured from the diffuser inlet plane (in)
Y	Diffuser inside radius (ft)

## 7.2 General Description

The output from DHTE is well labelled, and with the above nomenclature should be self-explanatory; however, a general description of the output should be useful to the first time user.

The initial set of information generated by DHTE consists of a user-defined title for the analysis followed by a listing of the user supplied input data.

At this point DHTE will read and organize the data contained in the first SCP2ND tape and will then call TBL. The next several sets of output information originate from within TBL. The first of these sets of information will be a set of boundary layer parameters, most of which were supplied by the DHTE input file. Stagnation temperature was supplied by the SCP2ND tape. This will be followed by a set of geometric data (radius vs axial location) for the diffuser along with edge condition Mach number and diffuser wall temperature. Following this will be a table of edge condition pressure,

temperature, velocity, and density data for use by the boundary layer analysis.

At this point, DHTE will perform a number of preliminary calculations and output preliminary data that will include M1, RE, V, HC1, C1, SCIPPY, KRPIK, DP(J), R(M), R1, R2, A, M2, and C2. During the listing of this information, DHTE will perform a check on the various stability criteria and print a warning message if any are being violated.

DHTE is now ready to begin the main heat transfer analysis. The initial condition listing that appears at this point is quite comprehensive, and includes numerous parameters that will remain constant throughout the analysis or until the next SCP2ND tape is read. Information will be listed at every axial station, and will include X, MDOT, SINE, DEBRIS, DEBRIS FACTOR, WALL EROSION, LINER EROSION, MDOTW, QPIJ, DELTA, HG, QHG, QPI, QPR, QHC, TAW, T, and TC. It should be noted that the wall temperatures are labelled as WALL TEMP and are listed sequentially from the gas side wall temperature to the water side wall temperature. Following this initial listing, the frequency of the output is controlled by the parameter DOUT and the output is appreciably abbreviated unless a new SCP2ND tape has been called, in which case the more comprehensive listing is triggered.

## 8. SAMPLE PROBLEM

### 8.1 General

DHTE has been used to analyze three Super BATES firings conducted at AFRPL Area 1-42. The 3 December 1982 firing will be presented here as a sample problem. The results of the analysis, along with a comparison of the DHTE predictions and the experimental data from all three firings, will be discussed separately under Results.

### 8.2 Preliminary Calculations

Most of the input information required by DHTE is available directly from the statement of the problem. The radiation source strength, however, is hand calculated from Equation 5. The mass flow rate for Particle Group 2 is



obtained from the output of SPP while the centerline velocity and temperature are obtained from the output of SCP2ND. From Equation 5

$$q = 3 \dot{m}_p \epsilon \sigma T_p^4 / U_p \rho_p R_p$$

$$\dot{m}_p = 16.46 \text{ lb}_m/\text{sec}$$

$$U_p = 8469 \text{ fps}$$

$$T_p = 4172 \text{ deg R}$$

$$\rho_p = 248 \text{ lb}_m/\text{ft}^3$$

$$= 0.1714 \times 10^{-8} \text{ B/hr-ft}^2\text{-R}^4$$

$$= 0.25$$

$$R_p = 9.829 \times 10^{-6} \text{ ft}$$

$$q = 86.3 \text{ B/sec-ft (per particle group)}$$

$$\text{KRPI} = 3 \times q = 259 \text{ B/sec-ft}$$

### 8.3 Input Data

The following data is necessary in order to run the program:

DX	= 1.0 in	
DTAU	= 0.05 sec	
DXMAX	= 1.0 in	(normally chosen equal to DX)
NDTAU	= 100	(this will provide 5 seconds of data)
NDY	= 7	
NCH	= 4	
DOUT	= 20	(this will provide data every second)
DCALL	= 80	(this will update TBL just prior to the end of the run)
NSCIP	= 1	(this provides for using only one SCP2ND tape)
DAFLAG	= 1	(set equal to nonzero this will provide for the storing of data sets)
DDAOUT	= 10	(data will be stored every 0.5 seconds)
DMXBA	= 1	(data will be stored every inch)
NDATA	= 2	(data will be stored as a function of time at two axial locations)
MDATA(N)	= 40, 56	(data will be stored as a function of time at 38 and 64 inches, (MDATA-2) x DX)

TKW = 0.5 in  
 WIDTH = 5.25 in  
 HT = 2.75 in  
 RHOW = 490 lb<sub>m</sub>/ft<sup>3</sup>  
 RHOC = 62.4 lb<sub>m</sub>/ft<sup>3</sup>  
 SPHTW = 0.1 B/lb<sub>m</sub>-R  
 SPHTC = 1.0 B/lb<sub>m</sub>-R  
 KW = 0.00863 B/sec-ft-R  
 MU = 0.000759 lb<sub>m</sub>/ft-sec  
 EROCW = 7.62 x 10<sup>-12</sup> ft-sec<sup>2</sup>/lb<sub>m</sub>  
 EROCL = 3.39 x 10<sup>-10</sup> ft-sec<sup>2</sup>/lb<sub>m</sub>  
 DISCH = 1500 gpm  
 XMOTOR = 12 in (the exit plane of the motor is positioned 12 inches in front of the diffuser)  
 XSTOP = 180 in  
 TI = 503 deg R  
 ACN = 1.0  
 ACP = 0.0  
 ACT = 0.25  
 TYPACN = 0  
 TYPDBR = 0  
 SCIP(K) = 11 (if more than one SCP2ND tape is to be called, this and all of the information to follow will be a sequence of NSCIP numbers)  
 ENDTBL(K) = 100  
 RBARK(K) = 77.37 ft-lb/lb<sub>m</sub>-R  
 (based upon a perfect gas assumption and a molecular weight of 19.97 obtained from SCP2ND)  
 PRK(K) = 0.473 (from SPP)  
 ZMOUK(K) = 0.00006541 lb<sub>m</sub>/ft-sec  
 (from SPP but adjusted for a stagnation temperature of 7043 deg R as obtained from the SCP2ND tape)  
 ZMVISK(K) = 0.660 (from SPP)  
 GAMOK(K) = 1.29 (from the SCP2ND tape)

PHIIK(K) = 0.001834 ft  
(from DWBLI)  
THETAK(K) = 0.001834 ft  
(from DWBLI)  
KRPIK(K) = 259 B/sec-ft

#### 8.4 Execution of Supporting Codes

SPP. SPP must be executed using the ODE and TD2P modules. No use will be made of the exit plane summary, but its inclusion should be of interest to the user. The output from the SPP run must be stripped of all information prior to the SPP banner that reads "\*\*\*\* SOLID PERFORMANCE PROGRAM (SPP) - VERSION n,nn \*\*\*\*" and cataloged in such a manner that it may be accessed by SPFI. The nozzle geometry is part of the input to SPP and is passed to SCP2ND by way of SPFI.

SPFI. The output from SPP must be attached to SPFI as TAPE7 along with two input files. A file of default inputs must be attached as TAPE4. This default file does not change problem to problem, except to the extent that SPPVER = '4A' must be included when using SPP Version 5 and deleted altogether when using SPP Version 4. A small file of specific input data is supplied to SPFI as TAPE5. Diffuser geometry is input through this file, passed on to SCP2ND, and subsequently passed on to DHTE. SPFI produces an output file TAPE1 that must be cataloged for use by SCP2ND.

The statement contained within the introduction to the effect that the code will run for a particle free flow must be qualified at this point. SPFI is the necessary link between SPP and SCP2ND; however, SPFI will not read the SPP output unless the tables that contain particle information are present. Therefore, it is impossible to run the code routinely for a particle-free flow. It is, however, believed that once Version 5 of SPP is fully operational, it may be possible to add a trivial solid content to an otherwise particle-free flow and make use of the codes. The statements that were added to SCP2ND to create the edge condition file for use by DHTE are believed to be capable of operating correctly with NPG=0 in the event that SPFI is modified or should the user wish to create some other link between SPP and SCP2ND. Since SPFI is not functional for this case, it has been impossible to run a test case with DHTE for NPG=0.

SCP2ND. The output file TAPE1 from SPFI must be available to SCP2ND as SCFILE. The first time that SCP2ND is run it will calculate the flow field for the supersonic portion of the nozzle and then proceed to calculate the flow field within the diffuser. In the course of this run, SCP2ND will create a file SCP2IN2 that, if attached to SCP2ND as SCFILE during a subsequent SCP2ND run, will allow SCP2ND to be run without recalculating the nozzle flow. SCP2IN2 may be edited by the user prior to these subsequent runs to alter the diffuser conditions or other parameters involved in the run. The only difficulty encountered so far in the use of SCP2ND has involved the parameter RX. RX controls the integration step size within SCP2ND, and has a default value of 1.0. This has, in general, been too large and it has been necessary to reduce its value to the vicinity of 0.4. RX may have to be altered in order to obtain the initial nozzle solution. If so, this change is made in the input file supplied to SPFI. Changes of RX for use in the diffuser solution are entered by editing the SCP2IN2 file. In cases where the point of impingement is located less than one motor exit radius downstream from the motor exit plane, it will be necessary to edit the SCP2IN2 file and rerun SCP2ND. In this case, the output from the SCP2ND run will supply the specific changes that must be made but leaves it to the user to realize that the changes are to be made within the SCP2IN2 file.

During the course of the diffuser calculation, SCP2ND will create information that will be required by DWBLI. This information will be supplied in two locations. SCP2ND will create a file called AEDCINV that must be cataloged for use by DWBLI. In addition to AEDCINV, there is a listing of data that appears at the end of the SCP2ND output that must be entered into a data file and made available to DWBLI.

As supplied, SCP2ND does not create a file of edge condition data for use by DHTE. The AFRPL version of SCP2ND has been modified to include this capability, and the information is written to TAPE99. Along with the edge condition data, TAPE99 also contains the particle size information, thermal properties of the particles, the motor exit radius, and the diffuser geometry which are input to DHTE. In addition to this information, TAPE99 contains additional information which should be useful to the user. Interpretation of the information contained in TAPE99 is best done in consultation with the WRITE statements contained within SCP2ND (these are contained within the

SCP2CT and SCP2IN modules, and carry the identifier 24NOV84) or the READ statements contained within MAIN of DHTE.

DWBLI. The output file AEDCINV from SCP2ND must be available to DWBLI as TAPE3 along with a file of data from the SCP2ND output which must be available as TAPE5. DWBLI will output a listing of boundary layer data among which will be the momentum and energy thicknesses to be used by DHTE as initial conditions for TBL.

It should be pointed out that file designations are compiler sensitive and that all file names referenced here are those used as compiled at AFRPL.

### 3.5 Execution OF DHTE

At the time of execution, the input data listed under Section 8.3 must be available to DHTE as TAPE5 and in a format as specified in Section 6. Listed below is a set of such card information generated by DHTE. The results of this analysis, along with supporting experimental data, will appear in Section 9.

#### CARD 1

SUPER BATES - 03DEC82

#### CARD 2

1.0        0.05        1.0

#### CARD 3

100        7        4        20        80        1

#### CARD 4

1        10        1        2        40        66

#### CARD 5

0.5        5.25        2.75

#### CARD 6

490.0        62.4        0.1        1.0        0.00863        0.000759

CARD 7

7.68E-12 3.39E-10

CARD 8

1500.0 12.0 100.0 503.0

CARD 9

1.0 0.0 0.25

CARD 10

0 0

CARD 11

11

CARD 12

100

CARD 13

77.37

CARD 14

0.473

CARD 15

0.00006541

CARD 16

0.660

CARD 17

1.25

CARD 18

0.001834

CARD 19  
0.001834

CARD 20  
259.0

## 9. RESULTS

Output generated by DHTE and based on data presented in Section 8 is shown in Figures 5 through 7 along with experimental data from the firing. The 77-inch diffuser located in Area 1-42 is instrumented to record water side wall temperatures on roughly 2-inch centers for the first 7 feet of the diffuser. The diffuser is also instrumented to record coolant temperatures on roughly the same intervals, but the burn time of the Super BATES motor is only about five seconds and does not result in an appreciable rise in the coolant temperature.

Prior to discussing a comparison of the predictions from DHTE and the experimental data, it would be well to comment on the experimental data presented in Figure 5. The diffuser is instrumented to record water side wall temperature by means of thermocouples spot welded to the inner wall of the water jacket. The junctions are formed by spot welding the individual thermocouple wires to the steel wall and allowing the wall to become a portion of the thermocouple circuit. It was hoped that by so doing, it would be possible to locate the effective thermocouple junction at the surface of the diffuser wall. The thermocouple wires were then strapped tightly to the diffuser wall in an attempt to heat sink them to the wall and minimize the heat loss down the wires. It is felt that the data presented in Figure 5 indicate the success of this endeavor. These thermocouples are sited on two straight line paths along the diffuser axis. One of these paths, labeled LHS, is located roughly 45 degrees from the top and along the left hand side of the diffuser facing in the direction of the gas flow. The other path, labeled RHS, is located roughly 45 degrees from the top and along the right hand side of the diffuser. The data shown in Figure 5 reveals a definite biasing of the data in terms of the RHS data being hotter than the LHS data, but shows either set of data from a single side of the diffuser to be very self consistent.

This consistency among the data from a single side of the diffuser is felt to rule out experimental scatter and to validate the quality of the data. The bias seen between the LHS and the RHS is definitely real. The exact same trend can be seen in the data gathered from two other Super BATES firings and presented later in Figures 8 and 10. This same trend was also seen in an entirely different motor tested in the facility prior to the Super BATES firings. This left to right variation in the data could be explained in terms of a lack of symmetry within the water jacket, a lack of axial symmetry in the diffuser, or a misalignment of the test stand with respect to the diffuser. For the moment, however, it is real and measurements taken on the facility reveal no misalignment between the test stand and the diffuser.

Were the motor burn time of sufficient duration to result in a steady state temperature distribution within the diffuser, the information contained in Figure 5 could be used to validate the manner in which DHTE handles to various heat loads within the diffuser. The temperature distribution as X ranges from 20 to 60 inches is predominately the result of gas side convection. An examination of Figure 5 in this region shows a good fit between the model and the data. That the initial rise in the prediction coincides with the rise in the experimental data at X equal to 20 inches indicates that SCP2ND is placing the point of plume impingement properly. While the model overpredicts the heat load at the point of impingement, the data and the model are in good agreement elsewhere within the 20- to 60-inch range, and one must conclude that TBL in conjunction with the boundary layer thicknesses supplied by DWBLI is handling the gas side convection in an acceptable manner. It should be pointed out that while one would expect to see a spike in the heat load such as is indicated by the model at the point of impingement, this spike has yet to show up in any of the experimental data. The thermocouple sites in all cases span the point of impingement and on 2-inch centers should catch the point of impingement but have yet to indicate this phenomenon. The temperature distribution as X ranges from 60 to 100 inches is predominantly the result of particle impingement, and the fit of the data in this region is primarily controlled by the selection of the thermal accommodation coefficient ACT. The selection of ACT equal to 0.25 was based solely on the fit of this data. It will be seen, however, that this value of



ACT results in a relatively good fit in the case of the two subsequent Super BATES firings.

Figures 6 and 7 show the dynamics of the system and point out the shortcomings of Figure 5 in terms of validating the model. As can be seen from Figure 6, the rise time of the system is approximately 30 seconds and, therefore, the temperature distribution within the diffuser at the end of 5 seconds is anything but steady state. If one can assume that the model handles the dynamics of the system perfectly, then one can calibrate the model using data such as shown in Figure 5. The information shown in Figure 6 certainly suggests that the model is handling the dynamics of the system well but also points out the real need for experimental data on a motor having a burn time of at least 30 seconds. The information shown in Figure 6 is in a region where gas side convection dominates the heat load and is for a RHS thermocouple. That the experimental data shown in Figure 7 appear to be headed for a higher steady state temperature than the model should come as no surprise since this is in the region where we have always seen a bias between the LHS and RHS data.

Figures 8 through 11 contain information very similar to that contained in Figures 5 through 7 but for two additional instrumented firings. As can be seen, the results are totally in keeping with those of the 3 December 1982 firing and support the conclusions just drawn regarding the performance of the computer model.

Figures 5 through 11 tend to support the validity of DHTE and the suggested accommodation coefficients, however, until such a time as a body of steady state data is available, the use of DHTE to predict maximum diffuser temperatures should be viewed as having an appreciable uncertainty associated with it.

In as much as meaningful erosion constants, EROCW and EROCL, for the 1-42 diffuser are not available at this time, erosion predictions are not included in these results. However, using the values generated from the AEDC data DHTE predicts maximum erosion rates of 0.008 in/sec for the liner and 0.0002 in/sec for the diffuser wall, both occurring at  $X = 62$  inches, for the 3 December 1982 Super BATES firings.

## 10. RECOMMENDATIONS

There are four recommendations with respect to the use of this code.

1. For the time being the code should be used with the following accommodation coefficients but every effort should be made to monitor the experimental data and adjust these parameters as more information becomes available.

$$ACN = 0.8 \sin B$$

$$ACP = 0.0$$

$$ACT = 0.25$$

2. An effort should be made to obtain a body of erosion data for the 1-42 diffuser in order to obtain appropriate values for EROCW and EROCL and generate meaningful erosion rate predictions.

3. Every effort should be made to obtain experimental data for a motor having a burn time of at least 30 seconds so that the treatment of the heat loads may be validated under steady state conditions.

4. An examination of the experimental data contained in Figures 5, 8, and 10 will reveal that in all cases the hottest spot recorded in the diffuser has occurred at the last thermocouple site. While the model predicts that the diffuser temperatures will decline from this point on, it would be prudent to install additional instrumentation downstream of this region.

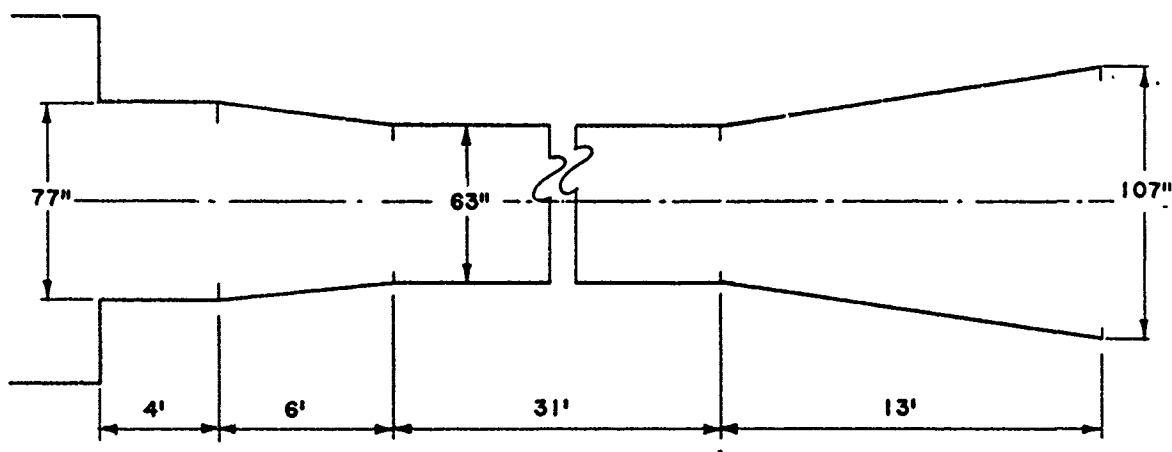


Figure 1. 77-in. Diffuser, AFRPL Area 1-42

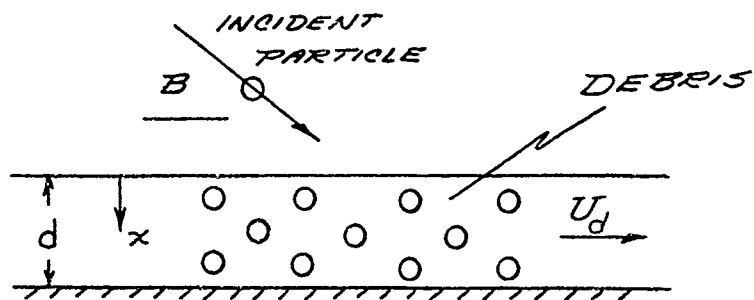


Figure 2. Debris Layer Model

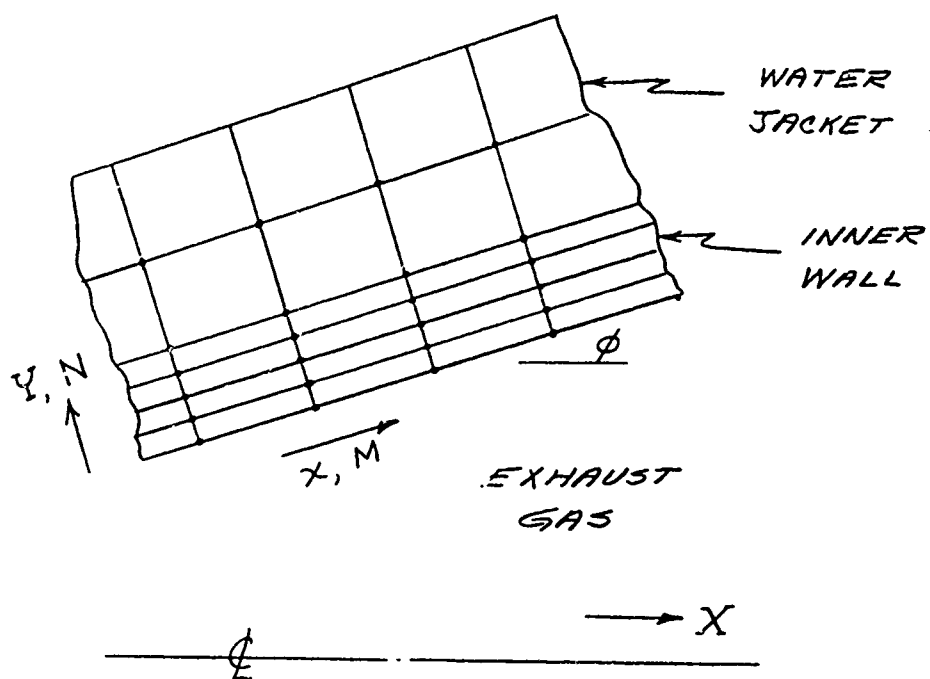


Figure 3. Finite-Difference Grid System

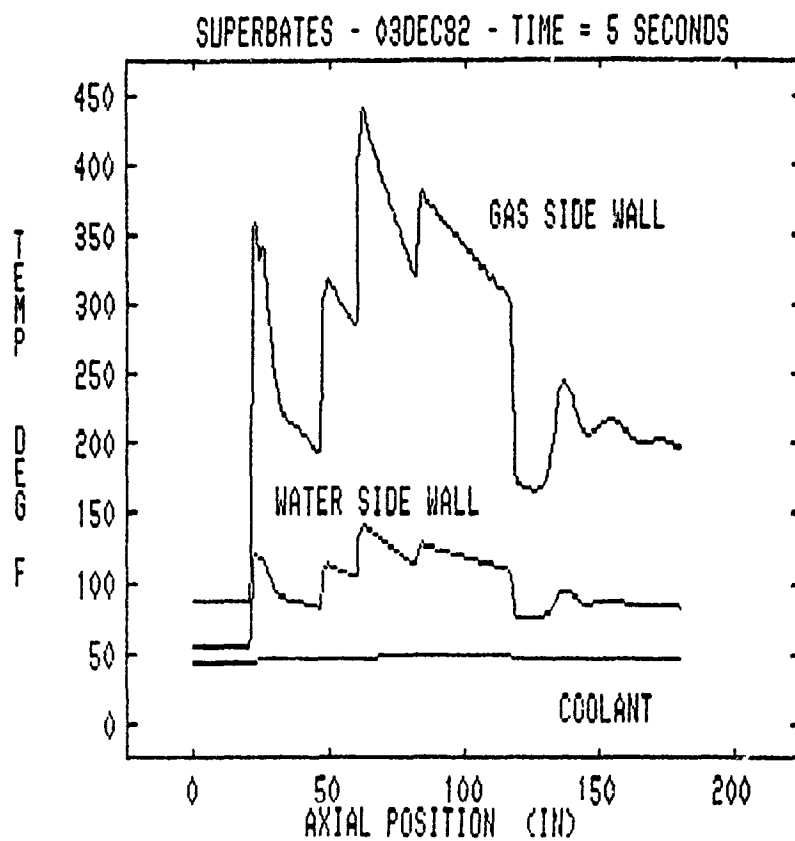


Figure 4. Axial Temperature Distribution

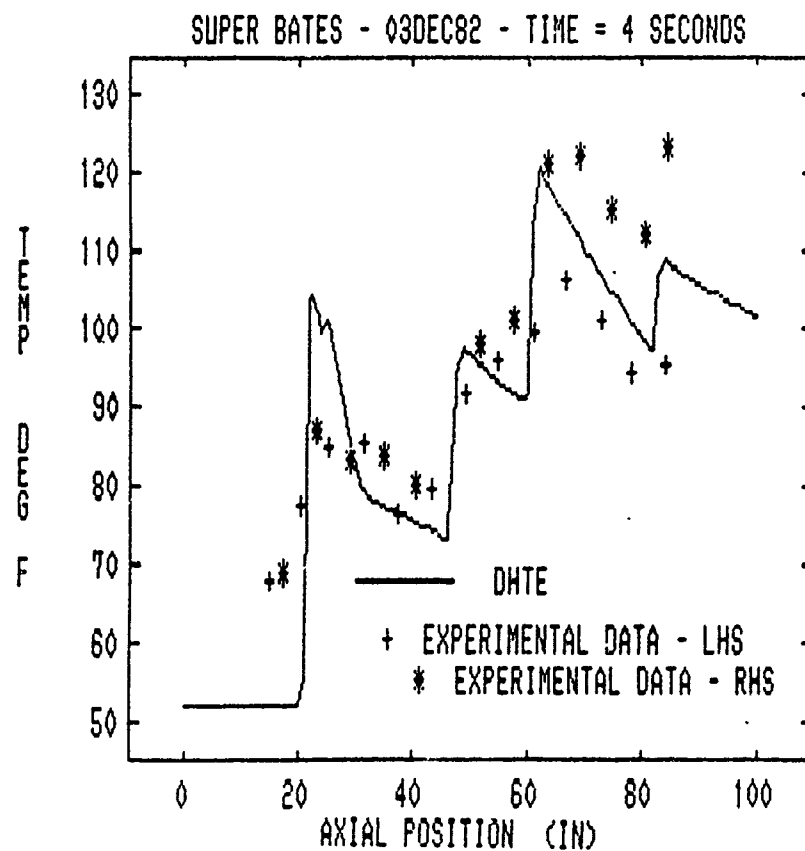


Figure 5. Water Side Wall Temperature as a Function of Axial Position, Super BATES, 3 December 1982

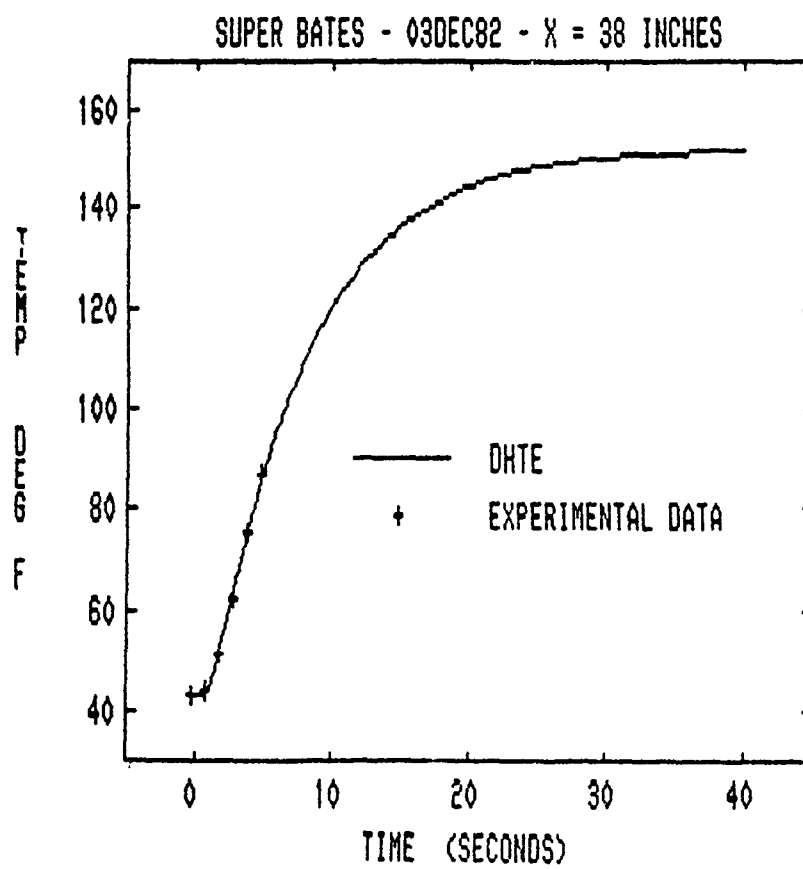


Figure 6. Water Side Wall Temperature as a Function of Time, Super BATES.  
3 December 1982

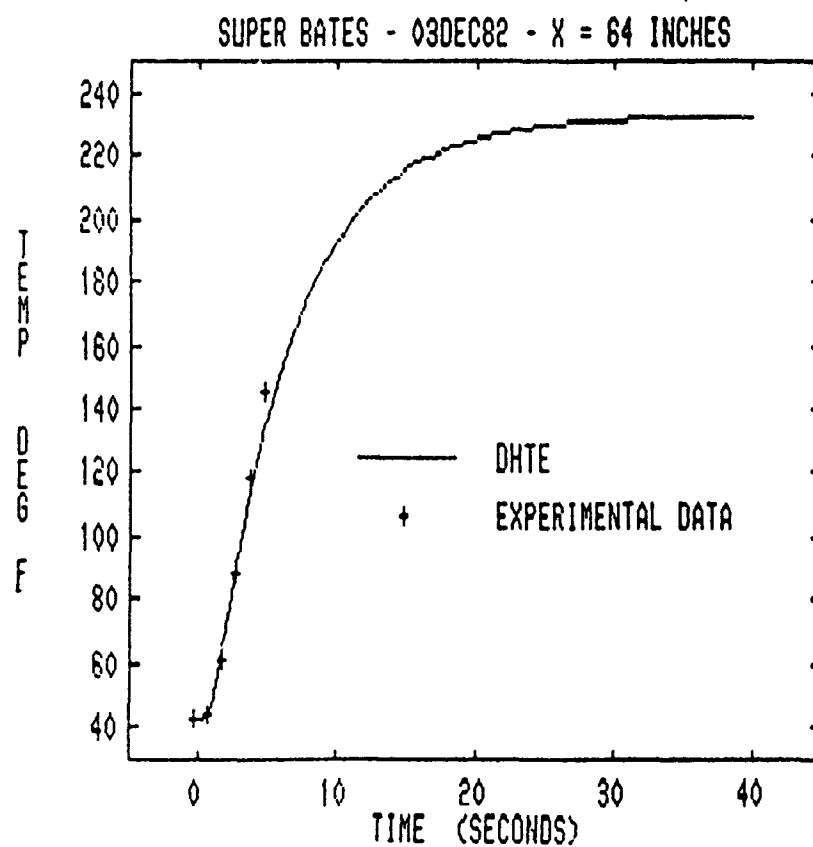


Figure 7. Water Side Wall Temperature as a Function of Time, Super BATES.  
3 December 1982



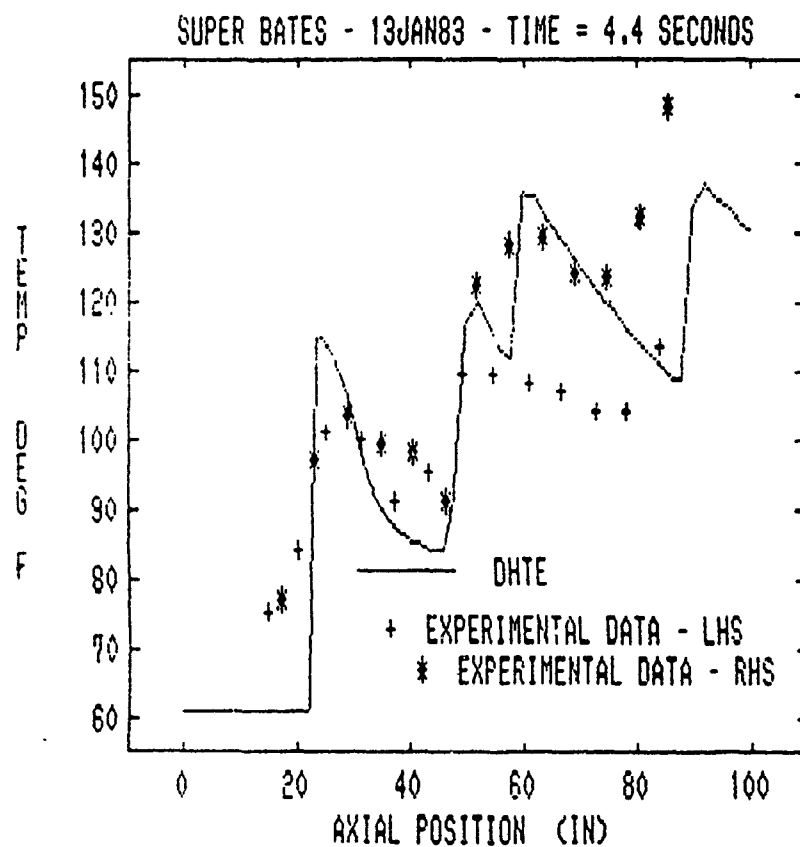


Figure 8. Water Side Wall Temperature as a Function of Axial Position, Super BATES, 13 January 1983

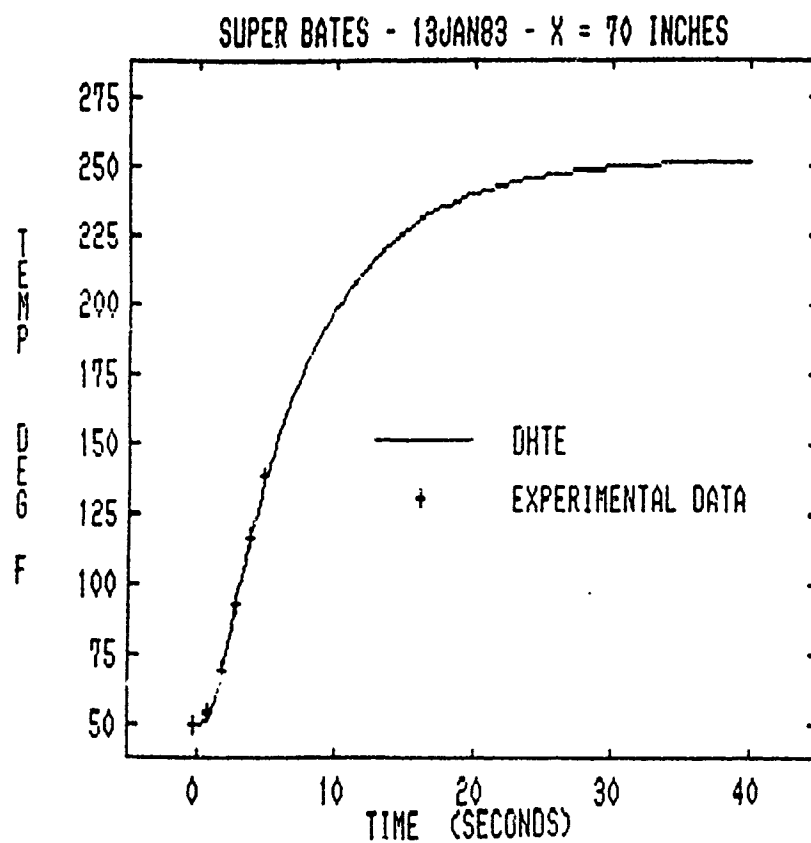


Figure 9. Water Side Wall Temperature as a Function of Time, Super BATES,  
13 January 1983

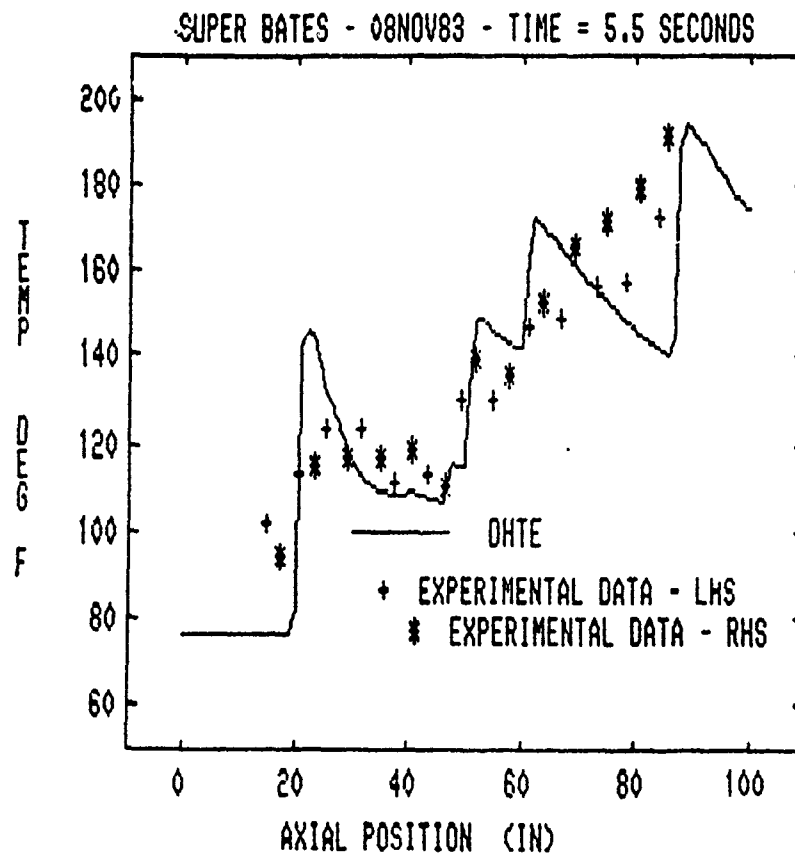


Figure 10. Water Side Wall Temperature as a Function of Axial Position, Super BATES, 8 November 1983

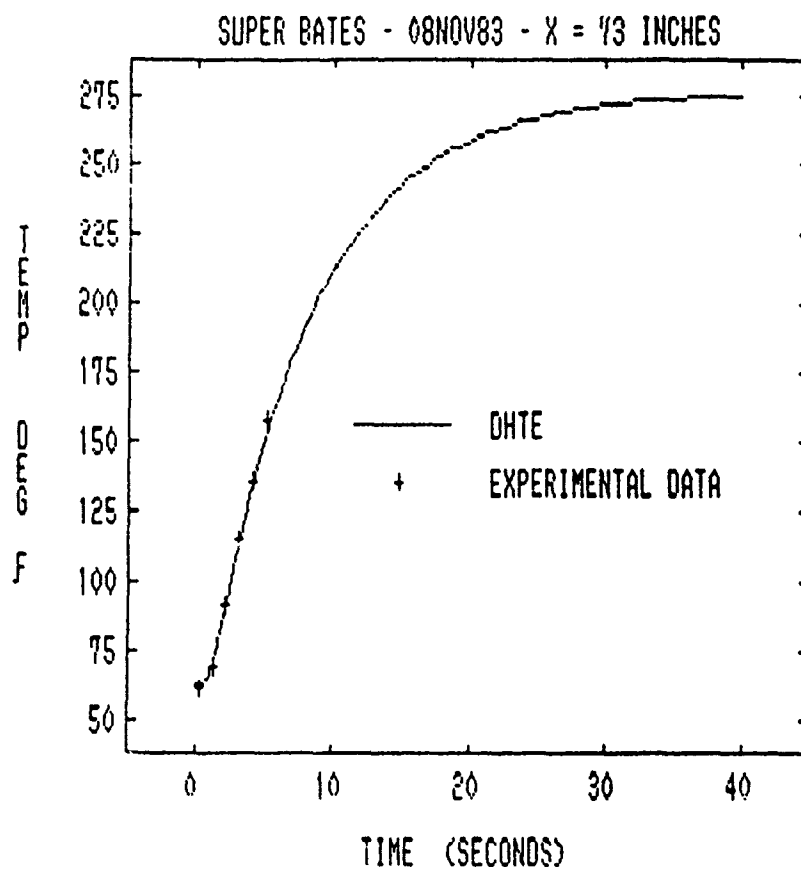


Figure 11. Water Side Wall Temperature as a Function of Time, Super BATES,  
8 November 1983

## REFERENCES

1. Trout, M. J., and McCay, T. D., "A Computational Model for Diffuser Analysis," AIAA 16th Thermophysics Conference, Palo Alto, Calif., June 1981.
2. Pergament, H. S., "Diffuser Heat Transfer Study," Final Report, Science Applications, Inc., Princeton, New Jersey, Redstone Arsenal Contract No. DAAH01-M-0330, March 1981.
3. Kessell, P. A., unpublished report.
4. Buzzard, G. H., A Diffuser Heat Transfer Code, AFRPL-TR-84-060 (AD-A149 270), November 1984.
5. Jordan, J. L., Girata, P. T., Simmons, M. A., Sherrell, F. G., and McGregor, W. K., Analysis and Measurements of Rocket Altitude Test Cell Diffuser Heat Transfer and Erosion, AEDC-TR-82-29 (AD-B076 968), September 1982.
6. Nickerson, G. R., Coats, D. E., and Hermesen, R. W., A Computer Program for the Prediction of Solid Propellant Rocket Motor Performance, AFRPL-TR-80-34, Vols. 1-3 (AD-B058 210, B063 541L, B058 243L), December 1980.
7. Wolf, D. E., Beddini, R. A., Dash, S. M., and Pergament, H. S., SPP/SPF Automated Code for Rocket Nozzle/Test Cell Diffuser Flowfield Calculations, AEDC-TR-85-29, Vols. I and II, May 1985.
8. Weingold, H. D., The ICRPG Turbulent Boundary Layer Nozzle Analysis Computer Program, NASA-CR-100653 (AD-841 202L), July 1968.
9. Wickman, J. H., Mockenhaupt, J. D., and Ditore, M. J., "An Investigation of Particle Impingement in Solid Rocket Nozzles," AIAA/SAE/ASME 15th Joint Propulsion Conference, Las Vegas, Nevada, June 1979.
10. Marks, L. S., Standard Handbook for Mechanical Engineers, 7th ed., McGraw-Hill Book Company, New York, 1967, Section 4.